Authors: Sebastian Borgs and Wolfram Stets, Institute of Foundry Technology, Düsseldorf

Porosity in ductile cast iron and its influence on the mechanical performance under cyclic loading

The highly complex solidification processes in ductile iron castings (GJS) may lead to non-optimal microstructures and volume deficits in casting practice. Shrinkage holes and micro-shrinkage porosity are among the most frequent defects in GJS. Depending on the distribution, size and position in the casting, these defects may negatively affect the mechanical-technological properties of castings. However, characterizing micro-shrinkage in destructive and non-destructive tests is problematic. Within the framework of a research project supported by AiF (German Association of Industrial Research Societies), the negative effect of increasing porosity on the mechanical properties of GJS samples was quantified

Especially in ductile iron castings, additions of steel scrap, pig iron, scrap iron or returns with elevated contents of tramp elements have a negative effect on the formation of the microstructure, e.g. through a non-optimal spheroidal graphite form, formation of pearlite or carbide, etc. [1]. Also the solidification behaviour may change such that there is a growing tendency of shrinkhole formation. These shrinkholes occur predominantly in the form of accumulations of micro-shrinkholes (see lead picture).

Moreover, the shrinkage behaviour of an alloy depends on its basic morphology of solidification. The solidification of ductile cast iron is predominantly endogenous with a mushy zone. To compensate liquid shrinkage, the solidification morphology requires interdendritic feeding (feeding through the interdendritic channels) [2]. As this feeding technique cannot always be guaranteed in foundry practice, porosity due to shrinkage is the consequence. If located in a critical area of the casting, depending on their size and distribution, shrinkholes may have a negative effect on the mechanical performance of a casting, resulting in a significant decrease in the service life. This holds particularly true for components subjected to cyclic stress in their field use.

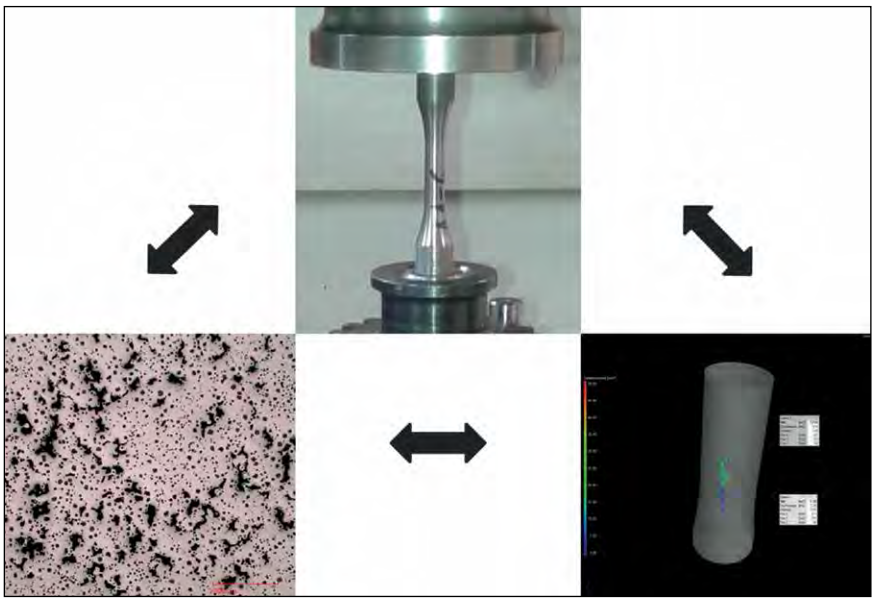

Correlation between cyclic properties and 3-D and 2-D porosity distribution in ductile cast iron (Photos and graphics: IFG)

The basis for dimensioning a ductile cast iron component according to its future field use are the static and, above all, cyclic mechanical properties stipulated in the applicable standards (DIN EN 1563) and in material data bases and guidelines. To date, the common practice of dimensioning and designing ductile iron castings for their specific field use has been limited to the use of (cyclic) performance data without considering internal defects. There is a lack of information about correlations between the quantity, size and distribution of shrinkholes and the static and, especially, the cyclic mechanical properties. This holds true, last but not least, for the ferritic high-Si GJS grades.

However, quantifying micro-shrinkage in destructive and non-destruc-

*Unless otherwise stated, the indicated percentages are mass fractions.

Alloy designation	Alloy no.	Contents of chemical elements in %*		
		Si approx.	P max.	Mn max.
EN-GJS-500-14	5.3109	3.8	0.05	0.5
EN-GJS-400-15	5.3106	2.4	0.03	<0.25

Table 1: Reference values for the chemical composition of alloys EN-GJS-500-14 and EN-GJS-400-15 according to [5] and [6].

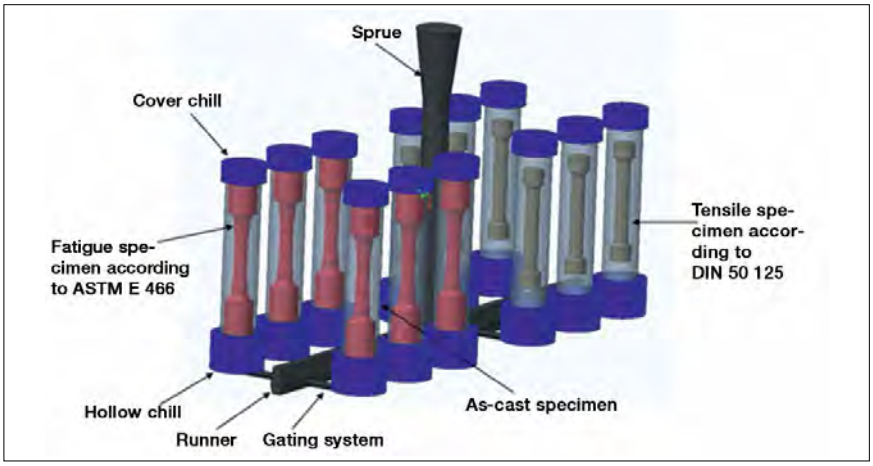

Figure 1: Casting system for making the test pieces for the specimens; specimens with shrinkage porosity were cast using cover and hollow chill made of EN-GJL-250. Specimens for the mechanical material tests (fatigue and tensile tests) as indicated

tive tests is problematic. Shrinkholes are usually detected by non-destructive ultrasonic or radiographic tests. However, these methods are still hardly or only insufficiently able to allow a quantification based on the size, ratio or distribution of the defect. A common practice to account for the influence of real microstructures (i.e. containing deviations in the microstructure and micro-shrinkage) on the strength of GJS components in a rather generalist way is to apply safety factors [3]. Safety factors applied to the yield strength may be as high as 2.1, depending on the stress load and the risk potential of the component [4]. For materials featuring an elongation at fracture A5 < 12.5 %, they may be even higher.

As the correlations between the distribution of micro-shrinkage in the casting and the cyclic mechanical performance values of GJS are still largely unknown, it may happen that despite the application of safety factors a component must be downgraded.

A key objective of the below described project was to determine scientifically profound correlations between the static and cyclic mechanical properties and the 2-D and 3-D distribution of porosity (micro-shrinkage) in cast GJS samples. The porosities were characterized using 2-D X-ray tests, X-ray computer tomography and 2-D analysis of microsections. A major part of the project consisted in comparing and discussing the results of the 2-D microsection analyses and of the X-ray tomography with the mechanical performance values determined in the tests. A further objective of the project was to develop optimized procedures for the evaluation of CT data. Additionally, preparation and evaluation algorithms for the analysis of micrographs of the porosity distributions in GJS were to be developed.

Testing

Tested materials

This project focused on ductile cast iron according to DIN EN 1563:2012, namely the conventional ferritic grade EN-GJS-400-15 and the solid-solution strengthened grade EN-GJS-500-14. Reference samples (graphite of form V and VI according to EN ISO 945-1, metallic matrix predominantly ferritic) and samples with shrinkage porosity were cast and examined. The chemical compositions of these alloys, as specified in [5] and [6], are listed in **Table 1**.

Casting of the specimens

The specimens were gravity cast and machined at the Technical Centre of the German Institute of Foundry Technology (IfG) in Düsseldorf, Germany. The melt was produced in a 100-kW medium-frequency induction furnace. The basic melt for the casting tests consisted of 60 % commercial-grade foundry pig iron and 40 % steel scrap. The Si content was adjusted to GJS specifications by means of FeSi-90 and the C content by means of commercially available carburizing agents. The melt was treated with the Mg master alloy by the Sandwich-Method. Here the treatment ladle at the same time served as pouring ladle. To guarantee nucleation of the iron during solidification, 0.3 – 0.35 % of inoculants were added to the molten iron. The inoculants used were SMW 605 (containing Al, Ca, Re and Bi, manufacturer: SKW) and Superseed (containing Ca, Sr and Al, manufacturer: Elkem) both having a grain size ranging between 0.7 and 3 mm. The molds were designed as core packages made of H32 silica sand (new sand), using the Pep Set sand binding method.

Based on the results from preliminary tests, a casting system with cylindrical patterns (40 mm diameter, 210 mm length), allowing the integration of cooling chills was designed for the deliberate casting of specimens containing porosities. The cooling molds were made of EN-GJL-250. The casting system was designed for pressurized, up-hill casting. The casting system is shown in **Figure 1**, as well as the positions of the samples for the mechanical material tests. Pouring and solidification simulations were conducted in order to verify the suitability of the casting system and the

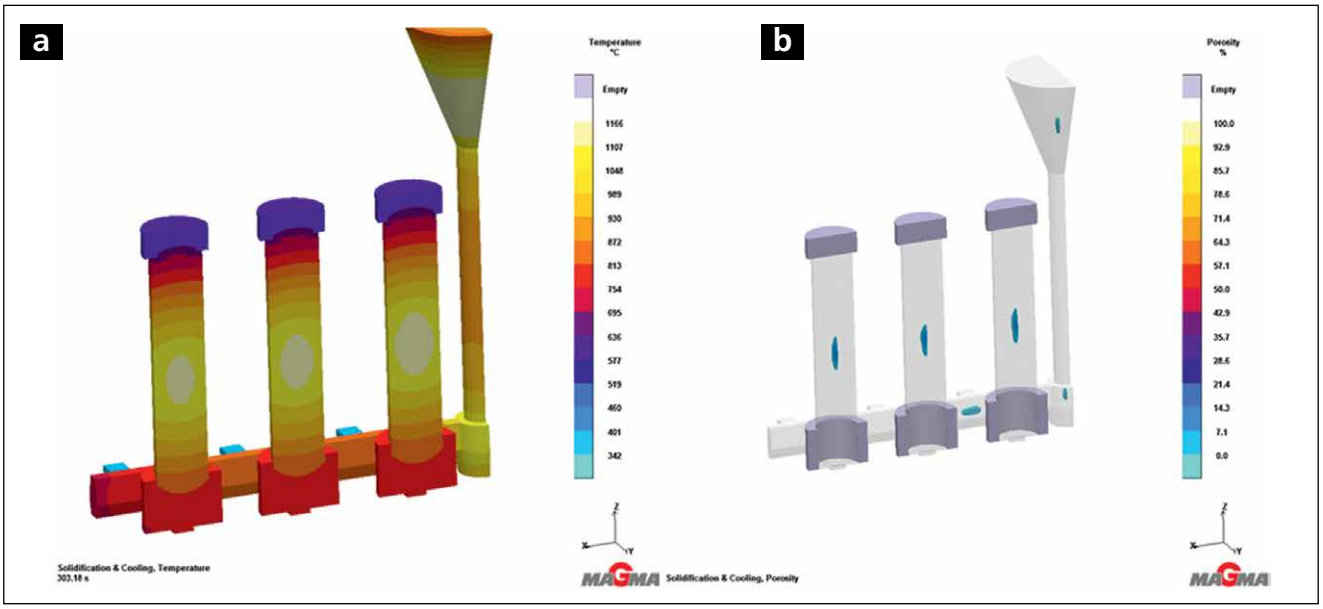

Figure 2: Results of casting and solidification simulation of the casting system shown in figure 1: a) temperature distribution after 303 s and b) predicted porosity in %

entire arrangement (**Figure 2**) for the intended purpose. It is clearly visible that by using the designed cooling chills (cover and hollow chill) the formation of porosities could be shifted to the central region of the cylindrical sample. With this arrangement, three porosity levels were produced with each alloy (36 cast bars of equal porosity level per cast heat). The different porosity levels were adjusted by applying suitable inoculation practices. In other words, certain inoculant ratios were applied while leaving all other casting parameters unchanged. The reference samples were cast as Y2 wedges according to DIN 1563. The chemical compositions are given in **Table 2**.

Alloy	Contents of chemical elements in %									
	C	Si	Mn	P	S	Cr	Ni	Cu	Mg	Sc
	Reference specimen									
GJS-500-14	3.11	3.7	0.09	0.01	0.004	0.04	0.046	0.019	0.05	1.02
GJS-400-15	3.5	2.4	0.09	0.01	0.004	0.04	0.046	9.019	0.042	1
	Porosity level 1									
GJS-500-14	3.2	3.78	0.089	0.01	0.007	0.051	0.052	0.016	0.05	1
GJS-400-15	3.42	2.5	0.079	0.01	0.003	0.03	0.05	0.02	0.045	1
	Porosity level 2									
GJS-500-14	3.1	3.6	0.081	0.01	0.003	0.029	0.041	0.015	0.043	0.99
GJS-400-15	3.39	2.36	0.066	0.01	0.003	0.03	0.05	0.022	0.043	0.97
	Porosity level 3									
GJS-500-14	3.1	3.67	0.086	0.01	0.003	0.031	0.047	0.02	0.053	1.01
GJS-400-15	3.4	2.44	0.079	0.01	0.003	0.03	0.05	0.02	0.043	0.98

Table 2: Chemical compositions of the cast specimens

2-D X-ray tests

Digital radiography was used for the 2-D X-ray tests. 100 % of the produced as-cast samples were tested. In each case, the radiographic tests were made from positions A and B. The X-ray parameters are detailed in **Table 3**. The X-ray images were evaluated using the ISAR evaluation software for digital radiography. This software allowed the measurement of the grey value profile of defects and the measurement of the length and width of renderable defects. Based on the X-ray tests, as-cast samples were selected for the subsequent examinations and categorized.

X-ray computer tomography

All samples evaluated in this project were tomographed by a Varian/BIR 450/225 kV-600 CT/DR system at a voxel resolution of 100 x 100 x 200 µm. As test method the fan beam technique (line scan detector) was applied using a section line distance of 0.1 mm. Based on the results from the 2-D X-ray tests a region of interest (ROI) of 50 mm was defined. For the scans, the settings listed in table 3 were used. The specimens scanned by CT were evaluated by means of the defect analysis module of the VGStudio Max2.2 evaluation software. The defect analysis feature contains a great number of different algorithms and analysis modes, which can be objectively set to obtain detailed information about any analyzed defect. As not all the evaluation algorithms of the software were equally suitable for the here investigated porosity, first the evaluation methods were optimized by means of a metallographic microsection. The position of some of the porosities were exactly measured in the CT data set and identified by targetted metallographic preparation. Based on the analysis of the 2-D microsections,

Testing method	Tube voltage in kV	Tube current in mA	Filter	Exposure time in s	Magnification	Dimension of focal spot in mm • mm	Voxel size (x, y, z) in µm	X-ray source
2-D x-ray	400	5	-	54	-	4.5	-	MG 420 (ROE 1)
CT	420	1.5	2 mm Brass	64 for 40 mm 32 for 15 mm	approx. 3	-	128 x 128 x 250	-

Table 3: Parameters of the X-ray tests

the threshold values for the detection of porosities were specified using VG-Studio Max 2.2 (grey value contrast, size, probability of porosity). With this technique it was possible to reliably determine whether any variations in grey values in the CT cross-sectional image are defects or CT artifacts. **Figure 3** shows a comparison of a metallographic microsection and the corresponding CT section. The circled areas in the metallographic specimen can be clearly related as porosities to the corresponding areas in the CT section. For the investigated shrinkage porosities, standard V.2.1 proved to be the best suitable evaluation algorithm. This algorithm comprizes multi-level image analysis techniques which are capable of identifying defects even if the grey value of the material and the contrast behaviour of the defect vary locally. When CT artifacts (e.g. ring artifacts) occur, it is possible to set analysis parameters in such a way that the defect recognition thresholds are partly reduced.

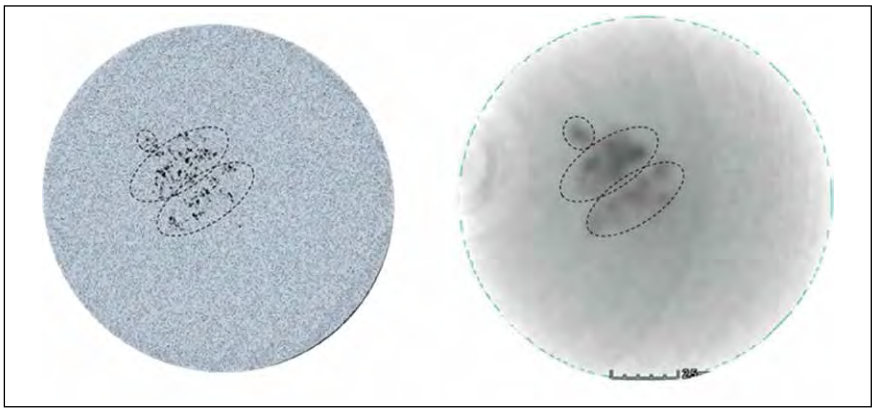

Figure 3: Comparison: a) metallographic specimen and b) the corresponding CT section

Mechanical material testing

Tensile tests

For the strength tests of the samples, a tensile testing machine of type Z 250 (manufacturer: Zwick & Roell) was used, subjecting the cross-section of the specimen to an evenly distributed linear tensile stress. The tensile strength tests were conducted according to specifications in DIN EN ISO 6892-1 with samples of shape B specified in DIN 50 125. The performance values tensile strength R_m, yield strength $R_{p0.2}$ and elongation at fracture A were determined.

Fatigue strength tests

The fatigue tests were performed with a high-frequency pulser of type Ru-

mul Testronic (manufacturer: Russenberger Prüfmaschinen AG). The testing machine features a nominal force of 100 kN and can apply frequencies between 40 and 250 Hz.

The fatigue tests were conducted under symmetrical load cycles with zero mean stress R = - 1. The samples were oscillated at a frequency of approx. 125 Hz. A sample was deemed broken when the oscillation frequency had fallen below 120 Hz or the output of the testing machine rose by 10 %. 107 cycles were chosen to represent the fatigue life. A combination of methods (staircase method + horizontal method) was used to determine the fatigue strength.

Additionally, investigations were made using the horizontal method at a constant stress amplitude of 230 MPa.

Samples according to ASTM E 466 were used as test specimens. The results were evaluated using the SAFD (statistical analysis of fatigue data) evaluation software.

The individual fatigue strengths were compared at 50 % probability of fracture.

Metallographic examinations

Scanning electron microscopic (SEM) examinations

The SEM examinations were conducted with a Hitachi S-3400N Thermo EDX & WDX scanning electron microscope allowing a maximum magnification of 30,000 x and a minimum magnification of 8 x (with SE detector). This instrument allows an up to 10 mm depth of focus. The fracture sur-

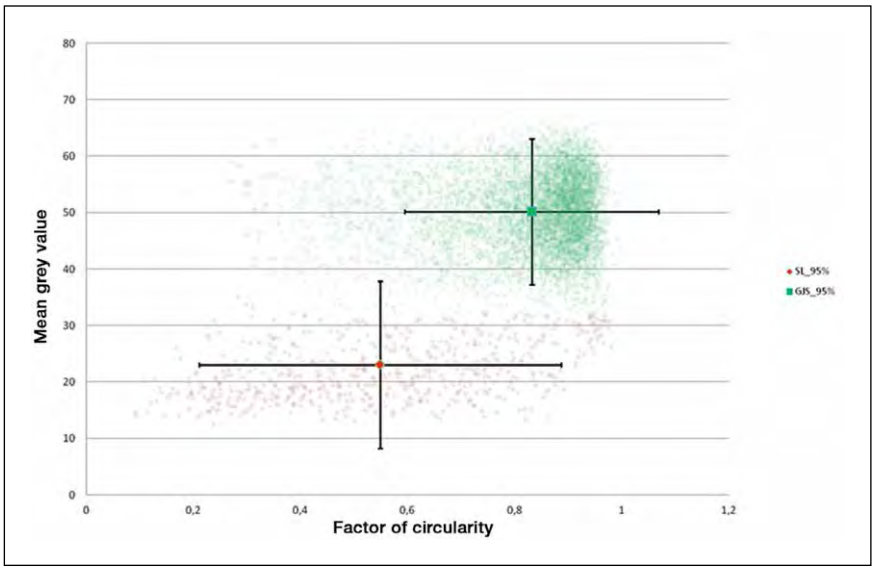

Figure 4: Mean grey value versus factor of circularity

Category	Feature	Min.	Max.
Porosity	Mean grey value	37	70
	Factor of circularity	0.25	0.75
	Area in µm	2,800 µm²	>2,800 µm²
Graphite	Mean grey value	10	37
	Factor of circularity	0.75	1
	Area in µm	20 µm²	2,800 µm²

Table 4: Determined category limits for object differentiation

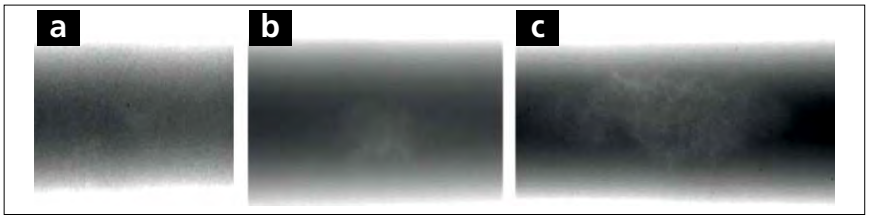

Figure 5: Results of 2-D radiographic tests: a) porosity level 1, b) porosity level 2, c) porosity level 3

Method	Porosity level	Length in mm	Width in mm	Volume in mm³	Surface area in mm²	Projection area in mm²	Porosity in %	Porosity in mm²
2-D x-ray	1	2.0 – 5.0	2.0 – 4.5					
	2	5.0 – 11.0	4.5 – 8.0					
	3	11.0 – 30.0	8.0 – 13.0					
CT	1			>0 - 80	>0 – 500	>0 – 50		
	2			80 - 215	500 – 1,670	50 - 90		
	3			215 – 1,200	1,850 – 4,600	90 - 150		
2-D microsection	1						0.1 – 3.0	0.2 – 5.3
	2						3.0 – 9.0	5.3 – 15.8
	3						9.0 – 18.5	15.8 – 32.6

Table 5: Classifications of porosity levels

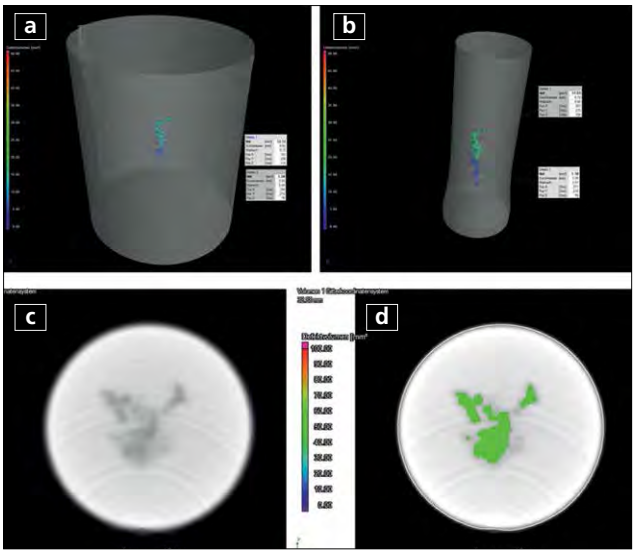

Figure 6: Results of the defect analysis of a specimen with porosity: a) as-cast specimen, b) specimen for fatigue tests, c) CT section prior to the defect analysis, d) CT section after the defect analysis

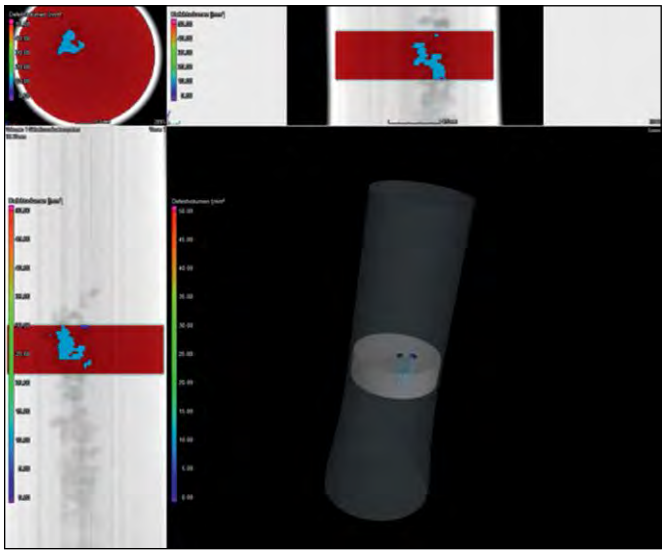

Figure 7: Example of a fracture region

faces of selected broken samples from the fatigue tests were examined by SEM to identify any crack-inducing factors such as porosities, inclusions and/or degeneration of graphite. Moreover, with the SEM it was possible to provide high-resolution images and evaluations of the characteristic fracture areas in a specimen broken due to fatigue failure (area of fraction due to fatigue failure and the residual fracture area).

Light-microscopic tests

The light-microscopic tests were made on unetched and etched metallographic microsections using a Zeiss Axio Imager.M1 microscope and a UI1460SE digital camera with a standard chip producing a resolution of approx. 2048 x 1536 pixels. The image analysis software dhs was used to evaluate the graphite including the metallic matrix. For the quantitative image analysis to determine shrinkage porosities (micro-shrinkage) an image analysis programme working with a motorized microscope table was used, in order to allow a maximum micrographic surface to be evaluated. A 2-D analysis of the microsections aimed at identifying porosities in ductile cast iron poses some problems because graphite nodules embedded in the microstructure have similar grey values as shrinkholes. Therefore, initially, the task was to define size and shape criteria allowing a quantifying analysis of the images according to the size, number and distribution of porosity. Following the sample preparation, characteristic microstructural images of micro-shrink-

age and spheroidal graphite were taken at a magnification of 100 (10x lense). If a sufficient digital resolution is available, the 100x magnification allows an exact analysis of the components in the microstructure. The characteristic parameters of the microstructure were determined by measuring the individual objects (shrinkholes and graphite) using the image analysis software Pixelferber. The obtained data were then exported to Microsoft Excel and contrasted with the determined features of the objects. This approach allowed to identify certain image-analytical features that differentiated from each other in specific respects. Especially data analysis based on the normal distribution proved to be a very successful method. The features with the smallest overlaps were later on used for the classification. The following features proved to be particularly suitable:

» mean grey value,
» factor of circularity and
» area.

In order to reduce the overlap of the normal distribution, both parameters referring to shape characteristics, i.e. mean grey value and circularity factor, were applied together. **Figure 4** shows the mean values (shrinkholes in red, graphite nodules in green) and a confidence region of 95 % for the mean grey value and the circularity factor. As a matter of course, the accuracy of the classification depends on the selected confidence region. A small confidence region leads to poorer accuracy, while a larger confidence region improves the accuracy, however, at the cost of a certain degree of overlapping of identification regions. The selected confidence region of 95 % still allows good distinction between graphite particles and micro-shrinkage. The interval limits were set based on the determined data. The category limits are summarized in **Table 4**. The classifiers or category limits were entered into the Pixelferber image analysis software. With the aid of a motorized cross table, the 2-D analysis of the microsections was carried out in parallel at the fracture surface of the tensile test samples and at selected samples from the fatigue tests. The microscope table

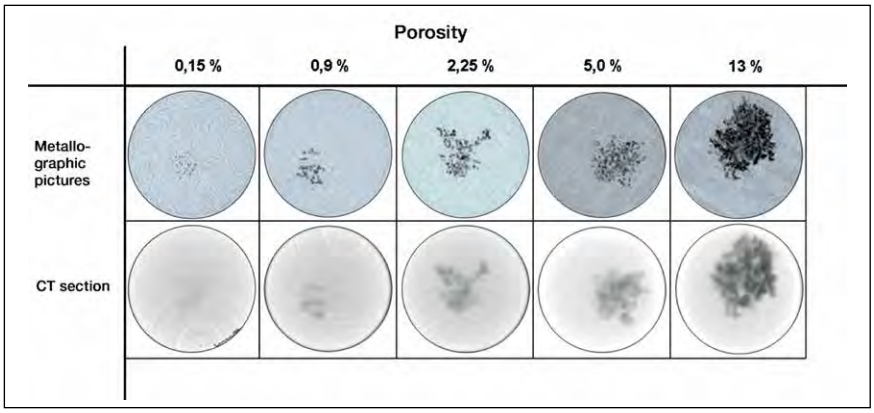

Figure 8: Metallographic specimens versus CT sections of the fatigue speci-

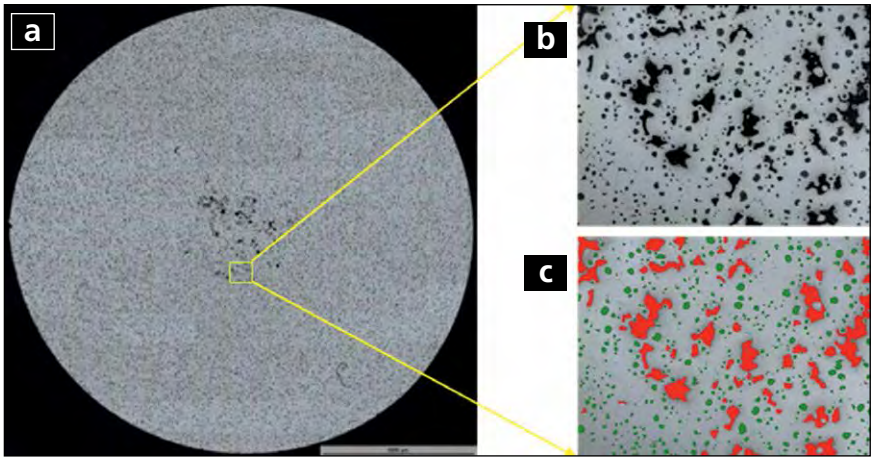

Figure 9: Results of a metallographic 2-D microsection analysis: a) panoramic view, b) single image prior to the image analysis, c) single image after the image analysis; red-colored areas are shrinkage porosities, green-colored areas are graphite nodules

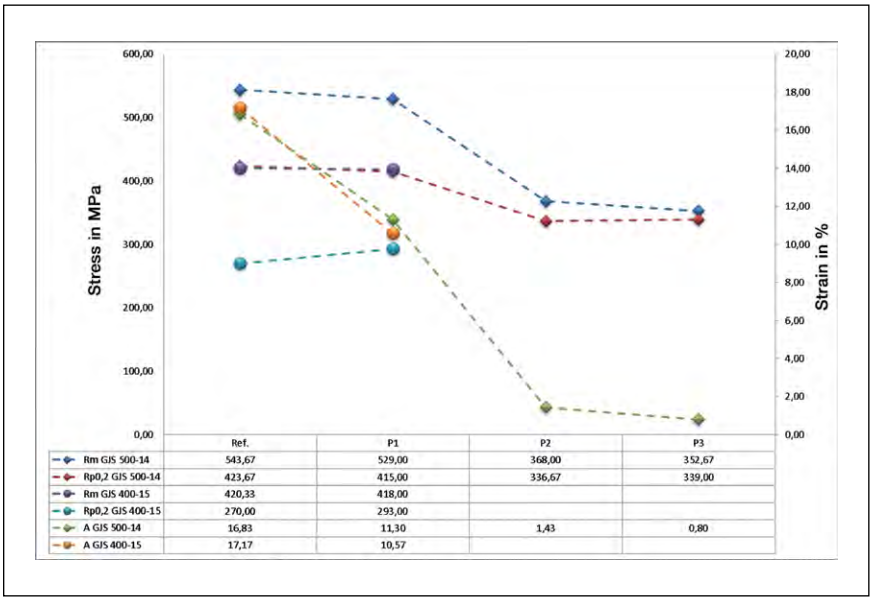

Figure 10: Static performance data of alloys EN-GJS-500-14 and EN-GJS-400-15 with and without porosities

and the Z-axis were both automatically controlled via the Pixelferber software. Especially the automatic steering along the Z axis ensures that the sample images are sharp over the entire area of measurement. The images were taken by a digital camera of type UI-1460SE and combined into a complete image (panoramic view) for the subsequent analysis, allowing also objects at the rims of the individual images to be captured.

Test results

2-D X-ray tests

Figure 5 shows results from X-ray tests of three different as-cast samples with varying porosities. Different grey value profiles and intensities are visible. They are the result of the varying absorption of the X-rays in the different regions. All phenomena shown correspond to defect class C of ASTM E-186, i. e. sponge-like shrinkage or disintegration of structure. **Table 5** shows the classification into three porosity levels. The analysis of the 2-D X-ray images revealed a relationship between the intensity of the voids (blackening ratio between defect and matrix) and the porosity level. Greater porosity resulted in greater intensity and better detectability. Detecting porosity levels 2 and 3 generally did not pose a problem. However, porosity corresponding to level 1 in terms of shape and distribution, were not detectable with sufficient reliability by 2-D X-ray tests. In some cases, the porosity could only be made visible by adjusting specific contrast settings via the analysis software. Nevertheless, reliable detection of porosities was not guaranteed.

X-ray computer tomography

The samples to be used in the CT tests were selected from the cast samples based on 2-D X-ray tests. They were scanned in the as-cast condition, i.e. 40 mm diameter, and then in the machined condition (as for fatigue testing), i.e. 15 mm diameter. Following criteria were selected for the defect analysis:

- volume in mm^3,
- surface area in mm^2 and
- area of projection in Z plane in mm^2 (cross-sectional area of the samples).

Figure 6 shows exemplary defect analysis results obtained by means of Volume Graphics from an analysis of as-cast and fatigue test samples. Figure 6a shows a porosity in the as-cast sample, and figure 6b in a fatigue test sample. In this case, there is exact correspondence between the as-cast sample and the fatigue test sample. The defects are shown in different colors depending on their size or volume. When the analysis has been completed, the defect size can be read from the included legend (defect volume [mm^3]). Figures 6 c and d show CT sections from a given plane in the specimen (2-D section) of a 15-mm-diameter bar – before and after the defect analysis by Volume Graphics. The classification into the three porosity levels is detailed in table 5.

Selected broken samples from the horizontal tests were used to measure the position of the fracture surfaces. Then, the defect analysis was made using the data of the thus measured fracture region in the set of data acquired during the CT tests of these samples. The fracture region was defined as having a length of 2 mm (1 mm from each fracture bank) and a diameter of 14 mm. Thus it is possible to analyze the porosity volume in the fracture region and correlate it with the cyclic performance data from the horizontal tests. **Figure 7** shows the fracture region of a specimen as an example.

Unlike 2-D X-ray tests, CT tests generally allow the detection of porosity level 1. A more detailed examination of the contrast distribution in a tomographic section (one voxel layer) reveals that if disintegration of structure (accumulation of many micro-shrinkholes) exists the resolution of the individual micro-shrinkholes is limit-

ed, which means that it is often only possible to examine a porosity region. **Figure 8** shows a comparison of CT sections and the corresponding, specifically prepared metallographic specimens. The images in the top row are the metallographic specimens, the images below are the CT sections. The metallographic specimens were evaluated using the developed 2-D analysis method. It immediately shows that while the sharpness of the metallographic specimens is good the CT sections are somewhat blurred. Moreover, the smaller the area of porosity, the poorer the detectability becomes, and vice versa: the detectability improves when the porosity is more pronounced. Porosity is sufficiently reliably detectable if the area is between 13 and 2.25 %. In case of porosity areas below 0.9 %, the detectability decreases significantly, while porosity areas of 0.15 % and below are no longer distinguishable.

The evaluation of the defect analysis revealed that areas of matrix material between the individual micro-shrinkholes had actually been classified as defects (see figures 6c and d). The result is a falsification of the real quantity and size of the porosity. In order to optimize the resolution, it would be possible to reduce the tube voltage from 450 kV to 225 kV or 180 kV. However, to achieve these lower tube voltages, CT systems with micro- or nano-focus tubes would have to be used. These CT systems are of smaller size, setting limits to the geometry of specimens that can be handled by the systems. Moreover, the maximum penetration depth is limited. According to [8], in iron-based alloys the maximum penetration depth of a 225 kV microfocus tube is approx. 30 mm, while a 450 kV macro-focus tube achieves a penetration depth of about 70 mm. In other words, many castings will be larger than the maximum penetration depth of the lower tube voltages.

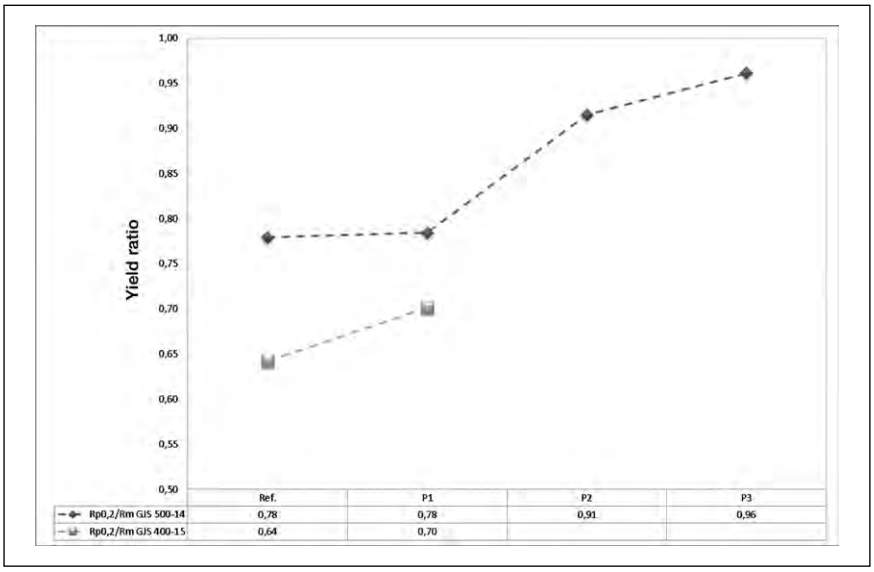

Figure 11: Yield ratios of the tested tensile specimens

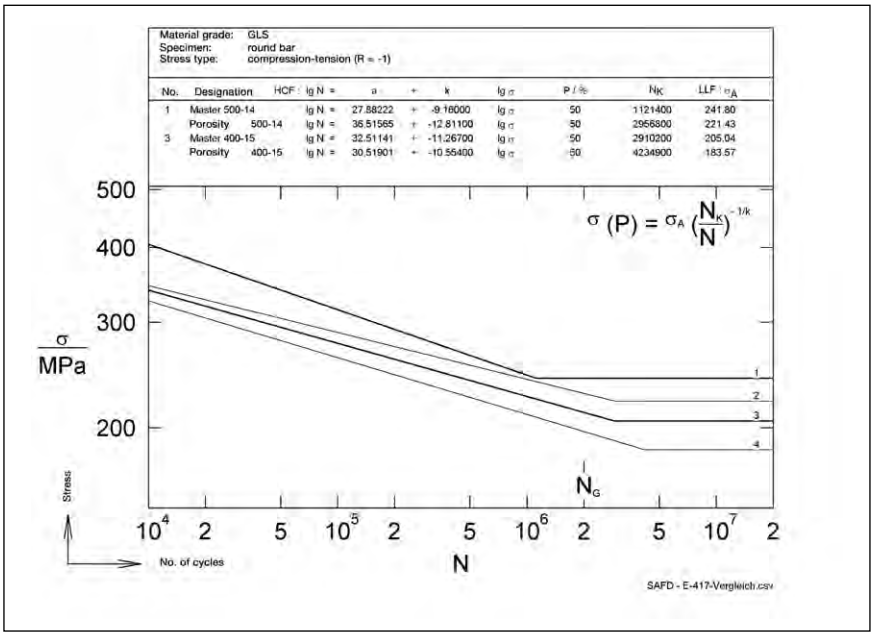

Figure 12: S/N curves of the tested specimens (probability of failure 50 %)

Metallographic 2-D analysis of microsections

The results from the analysis of the microstructure of ductile cast iron were, within a certain scatter band, comparable in all specimen types:

- graphite rate in the phase: 10.2 – 11.2 %,
- particle density: 310-352 1/mm^2,
- nodularity index: 75-82 % and
- ferrite/pearlite ratio: 98/2-94/6.

Figure 9 shows the result of a 2-D analysis of shrinkage porosity in a microsection. This example shows that the different components of the microstructure have been distinguished by different colours based on the results of the evaluation algorithms for the image analysis. Graphite nodules are shown in green and shrinkage porosity, the subject of this investigation, are shown in red.

The results from the classification into porosity levels by way of the 2-D analysis of the microsections are summarized in table 5. This proves that this is a reliable method, in terms of both quantity and quality, to analyze shrinkage porosity in ductile cast iron, however, presupposing a suitable preparation of the microsections. Ad-

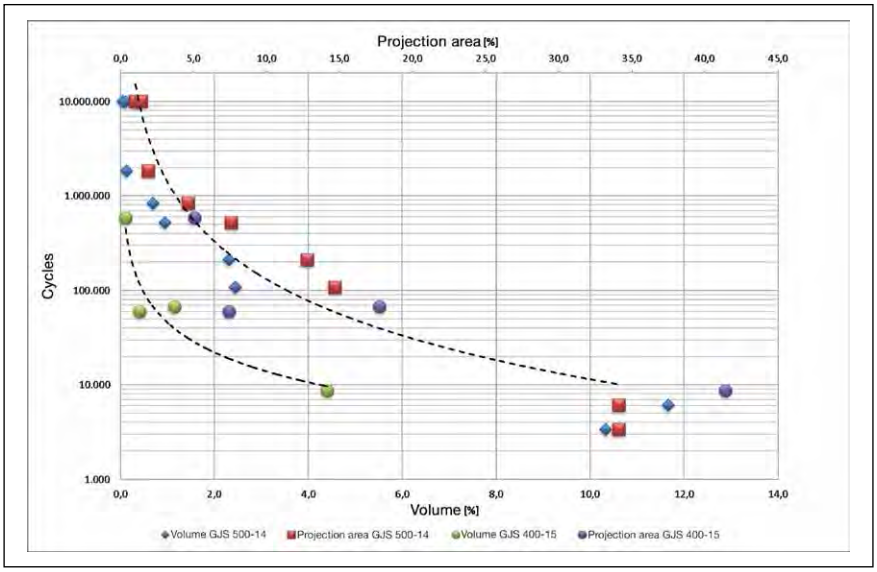

Figure 13: Effect of porosity (volume and area of projection) on the lifetime of the tested specimen (porosity determined by CT)

ditionally, certain overlapping of the characteristic features of shrinkholes and graphite nodules must be tolerated. However, it is possible to improve the accuracy by increasing the microscopic magnification. It would be possible to step up the magnification from 100 x to 200 x or 500 x, however, at the cost of a prolongation of the duration of measurement for the same measurement area.

Mechanical material testing

Static performance values

Figure 10 summarizes the performance values of the examined samples with and without porosity. The strength values (tensile strength and yield strength) of the Si-containing alloy (EN-GJS-500-14) are generally higher than those of EN-GJS-400-15. Only the elongation at fracture of EN-GJS-500-14 is slightly lower in the reference specimens. This is due to the different chemical composition and the significantly higher Si content. In EN-GJS-500-14, the higher Si content causes solid-solution strengthening of the ferrite. On the one hand, this leads to higher strength, on the other hand, it reduces the elongation at fracture. The static strength values of the samples of porosity level 1 did not decrease compared to the reference samples. The elongation at fracture is lower than in the reference samples by approx. 6-7 %. In contrast, the samples of porosity levels 2 and 3 are characterized by distinctly lower static performance values. The elongation at fracture slumps from 11.3 % to 1.43 and 0.8 %. Also the tensile strength and the yield strength - at 368 and 336 MPa respectively - fall short of the values stipulated in DIN 1563 for EN-GJS-500-14.

In ductile cast iron, the yield ratio plays a central role. The yield ratio is the quotient of the yield strength and the achieved tensile strength ($R_{p0.2}$/R_m). It indicates the elastic loadability of component. Of two materials having the same tensile strength but different yield ratios the one with the higher yield ratio can be more heavily stressed [9]. The yield ratio is also a parameter that may characterize the overload allowance of a material. A high yield ratio means a low overload allowance, that is, when the yield point has been exceeded only very little stress growth will be possible until reduction of area (plastic instability/component failure) occurs. For safety-critical components this bears the

risk that, in case of a high yield ratio, failure of the component will occur instantaneously once the yield point has been exceeded.

Figure 11 shows the yield ratios of the tested tensile samples of grades EN-GJS-500-14 and EN-GJS-400-15.

Like in the case of the static performance values, as described above, porosity also has an effect on the yield ratio. The yield ratio increases with increasing porosity. However, the rise is only significant in the case of porosity levels 2 and 3. Consequently, the overload allowance of ductile cast iron decreases with increasing porosity.

A highly critical aspect is the fact that this increase in yield ratio is the result of decreasing tensile strength and not of increasing yield strength with the tensile strength remaining at the same level.

Cyclic performance values

The S/N curves (50 % probability of fracture) of the reference specimens and of the specimens of porosity level 1 are plotted in **Figure 12**. The fatigue limit for alloy EN-GJS-500-14 is above that of EN-GJS-400-15 for both specimen types (see S/N curves 1 and 2 versus S/N curves 3 and 4). The higher Si content of alloy EN-GJS-500-14 has a positive effect on the cyclic performance values, similar to its effect on the static performance values.

Figure 12 also shows that the fatigue limit of the samples of porosity level 1 is about 20 MPa or 8 –10 % lower than that of the reference samples. This holds true for both alloy EN-GJS-400-15 and alloy EN-GJS-500-14.

Figure 13 compares the results from the horizontal tests (selected samples of alloys EN-GJS-500-14 and EN-GJS-400-15 subjected to a constant stress of 230 MPa) with the results from the defect analyses by means of Volume Graphics in the fracture region of the same samples (see figure 7). It is obvious that the fatigue limit decreases along with a growing porosity volume (3-D) and a growing projection area (2-D).

The influence of the area fraction of porosity (2-D) on the lifetime is also

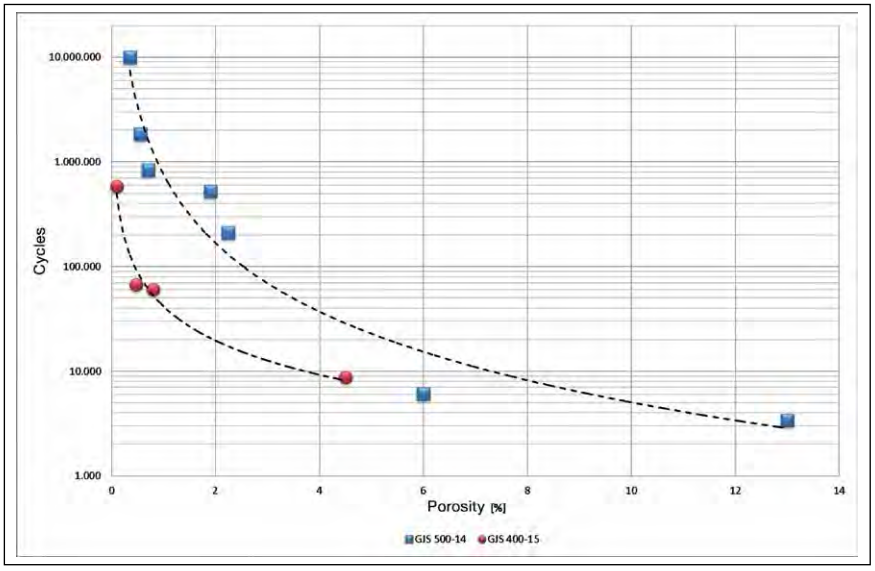

Figure 14: Effect of porosity on the lifetime of the tested specimen (porosity determined by 2-D microsection analysis)

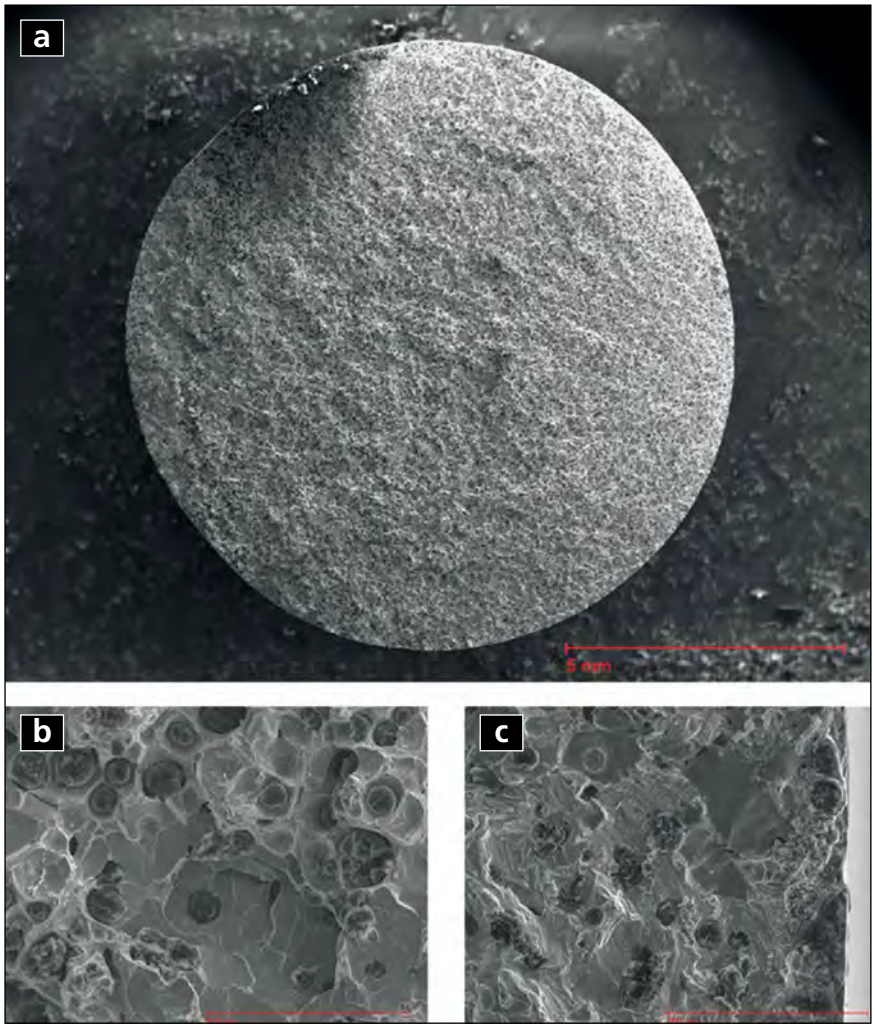

Figure 15: SEM analysis of fracture surface in an EN-GJS-500-14 reference specimen: a) panoramic view, b) residual fracture area, c) area of the fatigue crack / crack initiation

depicted in **Figure 14**. The fracture surfaces of the samples from the horizontal tests were examined by 2-D analysis of the microsections and set in relation with the endured cycles. Analogously with the curves in figure 13, the fatigue limit decreases with increasing porosity. The determined data points and the approximated curves of alloy EN-GJS-500-14 are generally at a higher level than those of alloy EN-GJS-400-15. This phenomenon is due to the higher strength values of Si-alloyed GJS. The barrier to fatigue crack initiation is higher.

From these test results it can be derived that the lifetime is most likely to be dependent not only on the porosity present in the fracture plane but that it also correlates with the porosity volume in the fracture region.

Fracture surface analysis

Figure 15 shows a fracture surface of an EN-GJS-500-14 reference sample from the S/N curve in the transition area. It was possible to determine the area of crack initiation (incipient cracking), the area of the fatigue crack and the residual fracture area.

In high-resolution images it was possible to show that especially in the residual fracture area of EN-GJS-500-14 there is a high fraction of transcrystalline cleavage fracture. EN-GJS-400-15, in contrast, shows mainly intercrystalline fracture of the common honeycomb-like pattern. While intercrystalline honeycomb-like fracture is characteristic of ductile fracture, transcrystalline cleavage fracture is characteristic of brittle fracture. These differences in fracture behaviour will have to be followed up on in future investigations.

In the fracture surface shown in figure 15, there is no characteristic feature in the microstructure that could be interpreted as crack initiator. **Figure 16** shows the fracture surface of an alloy EN-GJS-500-14 sample containing porosity. In the central area of the sample, zones of porosity and/or micro-shrinkage are clearly visible. From these zones, cracks propagate towards the sample surface. The residual fracture areas in the porosity-containing samples are very much like those in the reference samples. Also in this case, the solid-solution strengthened alloy EN-GJS-500-14 features a higher fraction of transcrystalline cleavage fracture than the conventional alloy EN-GJS-400-15.

In the reference samples, cracking initiates at the sample surface and propagates towards the centre of the sample. The cracks take semi-elliptical or pitch circle forms. From the results of the SEM analyses of the fracture surfaces it can be concluded that the cracks in the samples with porosities are predominantly enclosed internal cracks. The crack initiates in the existing micro-shrinkage, propagating towards the surface of the sample. Hence, the micro-shrinkage can be considered as the crack initiator. When the sample is subjected to stress, the lines of flux are diverted at the micro-shrinkage, causing the local stresses inside the specimen to rise. The local internal stress is higher than the stress acting on the sample surface. This explains why the internal cracking occurs first. **Figure 17** shows an image of a fracture situation in which the fatigue crack initiated at the surface of the sample although there was micro-shrinkage in the central area of the sample. This can be explained by the fact that there was a subsurface defect, which was more likely to initiate a crack than the micro-shrinkage in the sample centre.

Summary

The project involved the casting of samples of EN-GJS-400-15 and EN-GJS-500-14 ductile cast iron with and without porosities and their subsequent testing. First the shrinkage porosities were quantified and classified using 2-D X-ray testing and X-ray computer tomography. This was followed by static and cyclic tests of the reference samples and the samples containing porosities. The fracture surfaces of the broken sam-

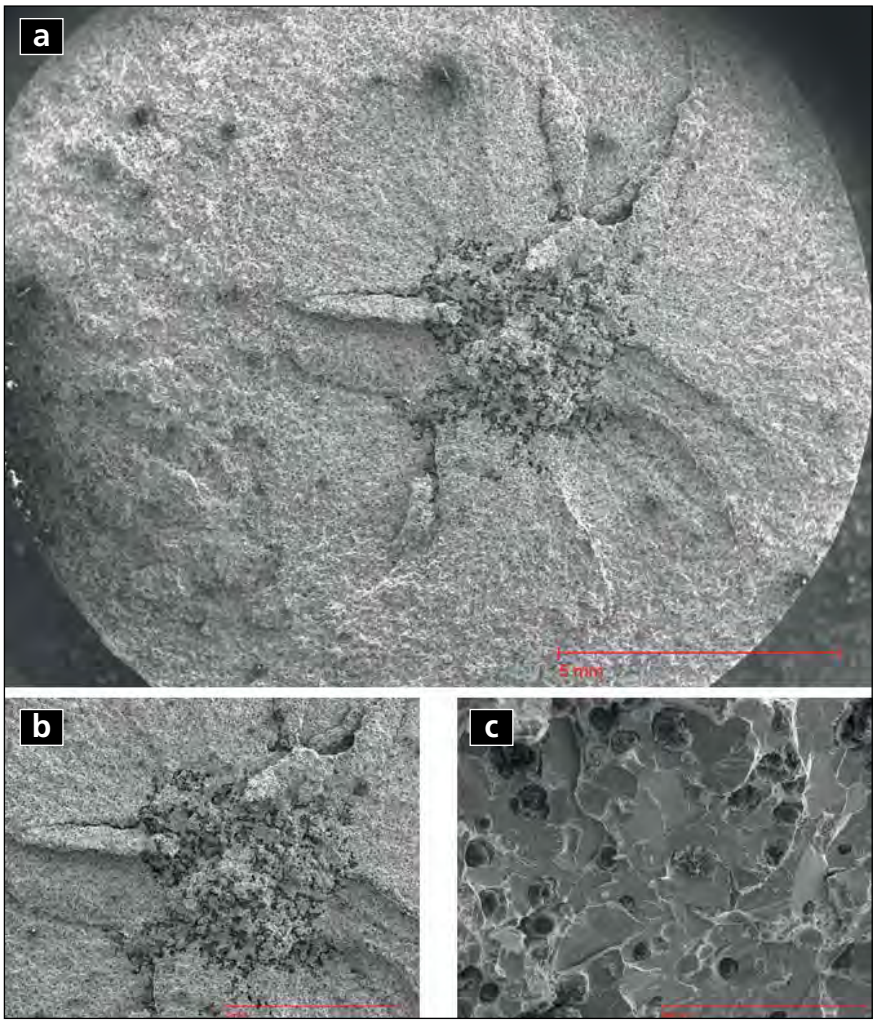

Figure 16: SEM analysis of fracture surface in an EN-GJS-500-14 containing porosities: a) panoramic view, b) porosity, c) residual fracture area

ples were analyzed by means of metallographic 2-D microsection analysis and SEM. The results from the porosity analyses were compared with the mechanical performance values and discussed.

Methods of characterizing shrinkage porosity

While the suitability of 2-D X-ray testing for detecting shrinkage porosity of level 1 in the as-cast GJS samples of 40 mm is only limited, this testing method has proved successful for accurately detecting porosity levels 2 and 3.

However, with X-ray computer tomography it is in most cases possible to also detect and quantify micro-porosity of level 1. The CT image allowed only limited resolution of individual micro-shrinkholes. Therefore, it was often only possible to examine the porosity region. Consequently, the defect analysis by Volume Graphics classified also areas of matrix between the micro-shrinkholes as defects. The result is a falsification of the real quantity and size of the porosity. Another finding was that detectability decreases with decreasing porosity. In samples of 15 mm diameter, for example, it is no longer possible to accurately detect porosities as low as 0.25 % or 0.44 m^2 (determined by 2-D microsection analysis).

For the prevailing porosity (disintegration of structure due to shrinkage through to pronounced shrinkhole accumulations) the Standard V.2.1 algorithm integrated in the defect analysis of Volume Graphics has proved as the most suitable evaluation algorithm in this application. Additionally, the results from the analysis of the metallographic microsections can be used to assess and calibrate the 2-D or 3-D information obtained from the X-ray tests.

Analyzing shrinkage porosities by means of the developed preparation and evaluation algorithms for image analysis has proved to be reliable in terms of both quantitative and qualitative accuracy. Therefore, this analysis may be used as a reference for the verification of other CT-based examinations. This method is also a suitable tool for the quality control of components made of ductile cast iron.

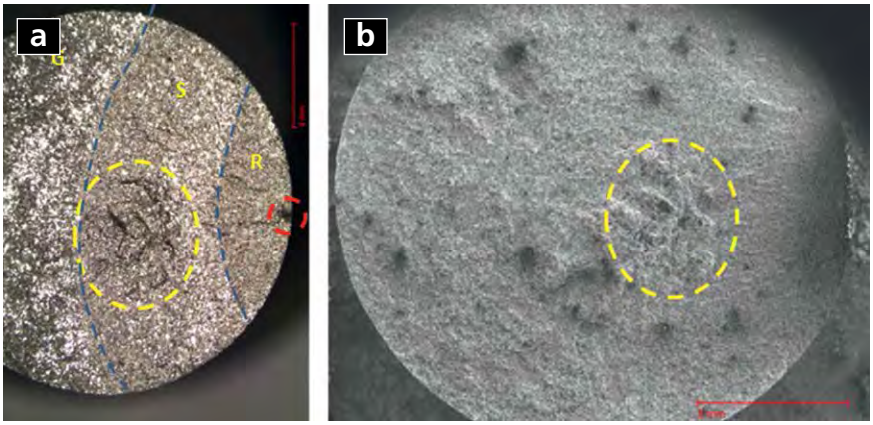

Figure 17: Fracture surface of an EN-GJS-500-14 specimen: a) stereomicrograph, R = crack initiation, S = crack propagation, G = residual fracture area; subsurface defect marked red, micro-porosity marked yellow; b) SEM image, micro-porosity marked yellow

Influence of porosity on the mechanical performance values

It can be summarized that there is a general effect of the here studied, deliberately produced shrinkage porosity on the static and cyclic performance of the casting. This holds true for both the solid-solution strengthened alloy EN-GJS-500-14 and the conventional ferritic alloy EN-GJS-400-15. Samples without defects (ideal condition) served as reference material.

The effect of porosity on the static performance first and foremost shows in a decreasing elongation at fracture. Samples of porosity level 1 did not exhibit any negative effect on the strength properties (R_m, $R_{p0.2}$). The strength values only started to decrease in samples of porosity levels 2 and 3. At these levels, the elongation at fracture is likewise negatively influenced.

The fatigue limit is about 20 MPa or 8-10 % lower than that of the reference samples. These figures are the same for alloys EN-GJS-500-14 and EN-GJS-400-15.

The fatigue limit decreases with increasing porosity, with the lifetime depending on both the porosity volume and the area of porosity in the fracture region.

Fatigue cracking may be initiated by micro-shrinkage. However, cracks may also initiate from surface pores or subsurface defects, although micro-shrinkage – even if representing a significant volume fraction - is present inside the sample.

The relationships between porosity and the performance of the materials under cyclic stress, which were identified as part of this project, are exclusively valid for fatigue tests with R = -1. Bending and torsional tests were not conducted.

The IFG project 17316 N of FVG Forschungsvereinigung Gießereitechnik e.V. (Research Society for Foundry Technology) was conducted under the sponsorship of the German Federal Ministry of Economy and Technology via the AiF (Association of Industrial Research Societies) within the framework of the Programme for Industrial Collective Research and Development based on a resolution by the German Federal Parliament. We would like to take this opportunity to express our thanks for this support. We also wish to thank the companies of the working group which accompanied and supported us during the entire project period of more than two years. Our special thanks go to the enterprises Iron Foundry Baumgarte GmbH, Bielefeld, Ford-Werke GmbH, Cologne, and Volume Graphics GmbH, Heidelberg, for their contributions to the project.

References:

www.cpt-international.com